Sensitivity Analysis of Fractal Dimensions of Crack Maps on Concrete and Masonry Walls

Amir Rezaie, Antoine J.P. Mauron, Katrin Beyer[*]

Earthquake Engineering and Structural Dynamics Laboratory (EESD), School of Architecture, Civil and Environmental Engineering (ENAC), École Polytechnique Fédérale de Lausanne (EPFL), EPFL ENAC IIC EESD, GC B2 515, Station 18, CH – 1015 Lausanne, Switzerland

Abstract

Assessing building damage after earthquakes requires a visual inspection of the damage, indicated by maps of the cracking pattern on walls, which could be standardized via automated algorithms. To quantitate this damage, fractal dimensions of these crack maps could be computed by the box-counting algorithm to capture the complexity and irregularity of the pattern. When using the box-counting method, however, the computed fractal dimensions depend on several parameters that can render the measurement ambiguous: the box size interval, the scale factor for the box sizes, the choice of breakpoint location, and the grid disposition and orientation. This paper, therefore, uses a literature search and an evaluation of crack map databases to investigate the sensitivity of the measured fractal dimensions of crack maps on reinforced concrete and unreinforced masonry walls to these four parameters. It then formulates recommendations for the choice of these factors. Because the value of the estimated fractal dimension varied by up to 0.5 depending on the assumed parameters, it is therefore important to use the same set of assumptions when comparing the fractal dimensions of crack patterns.

Keywords: Fractal; Box-counting Method; Crack Map; Concrete Walls, Masonry Walls.

---

[*] Corresponding author email: katrin.beyer@epfl.ch

1. Introduction

The first step in assessing the safety of buildings after earthquakes is a visual evaluation of the damage [1], which will likely be automated in the future through high-resolution cameras mounted on unmanned aerial vehicles (UAVs). This is currently done instead via an expert assessment of the appearance of cracks in structural elements to determine the extent of the damage and to understand the behavior mode of the element and the damage severity [1–3]. To successfully apply unmanned imaging techniques to this evaluation, however, the extraction of the damage pattern and the interpretation of the damage should be done automatically. Towards this end, various approaches have been developed to detect cracks on images [4–8]. To automatically interpret the extracted crack patterns and estimate the effect of the cracks on the properties of the structural elements, it is necessary to quantitatively characterize the crack pattern. When visually evaluating these patterns, physical characteristics of cracks, including the orientation, length, and width, are used [9,10]. When a visual inspection is replaced by image-based inspection, these crack characteristics can be complemented by other measures, such as fractal dimensions, which can only be evaluated using computational tools. A growing body of research in civil engineering involves investigating the applicability of fractal dimensions for characterizing crack patterns [11–20], as using fractal dimensions rather than a classical visual inspection can reduce the subjectivity of a visual assessment, which often depends heavily on the experience and expertise of the inspector [21,22].

The notion of a fractal can be traced as far back as studies in the 1800s to early 1900s by Hilbert [23]. However, it was Mandelbrot [28] in the 1980s who found that mathematical fractals have some common features with natural shapes [29]. The concept of fractal dimensions has been applied in a variety of research domains, including plant science [30–32], neuroscience [33], architecture [34], porous structures [35–37], crack maps [21,22,38], etc., and is being used as a quantitative approach to describe the complexity, irregularity, and space-filling of objects [28,30,31,39–41]. In general, there is not a universal definition of fractals [42], and different values of the fractal dimensions can be obtained for a particular set based on the applied concept [39].

In deterministic fractal geometries that are generated based on a construction process, like in **Fig. 1(a)**, a small portion of the pattern exactly resembles the larger portion (exact self-similarity) [42]. Real-life crack patterns, however, are only statistically or approximately self-similar, like in **Fig. 1(b)**. Although crack maps are not perfect fractals, the notion of fractal dimensions can still be used to describe them. For example, some recent studies relate the fractal dimensions of crack maps on both concrete and masonry walls to some structural properties, like stiffness loss, strength loss, and the peak drift ratios [21,22,38,43,44]. To compute each fractal dimension, there are various approaches, including box-counting methods, gliding box algorithm, fractal Brownian

motion, area measurement methods, wavelet methods, and so on [45,46]. All of these methods have some advantages and drawbacks, which may restrict their applicability to certain types of problems [45]. In addition to the classical fractal dimension, which shows the space-filling and complexity characteristic of patterns, further types of fractal dimensions have been put forward to describe other aspects of patterns on images. Among these are the lacunarity, showing the distribution of gaps in patterns [28,47], and the succolarity, representing the connectivity of the pattern [28,48], though these dimensions have not yet been used for characterizing crack patterns of structural elements and will not be discussed further in this paper.
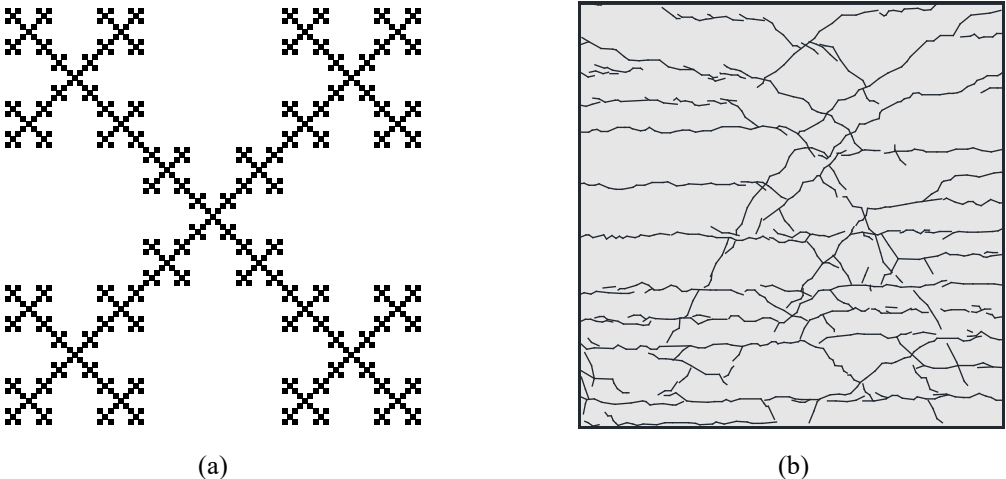

(a)   (b)

Fig. 1 Exact vs. statistical fractal.
(a) Box fractal (image adopted from [42]) and (b) a typical crack map on a concrete wall surface [49].

To evaluate the fractal dimension of crack patterns of structural elements [21,22,38,43,44], existing studies have used the box-counting method, which—due to its ease of calculation—is the most common [50]. When applying this method, several choices need to be made [33] related to the grid position and orientation with regard to the crack pattern, the box sizes used, and the box size interval over which a straight line is fitted to the resulting log-log graph, which relates the number of boxes that contain a pattern pixel and the size of the boxes. It has been demonstrated that slight changes in the considered methodological factors might lead to different fractal dimension estimations [31,32,34,51–58]. The objectives of this paper are (i) to investigate how sensitive the fractal dimensions of crack patterns are to these choices and (ii) to formulate some recommendations for these parameters. For this purpose, we review both the parameter choices in existing crack-pattern studies and recommendations for these parameters that have been made for patterns other than crack maps. For this purpose, we analyze crack patterns from reinforced concrete and unreinforced masonry walls. The paper begins with the definition of the fractal dimension and an explanation of the box-counting method. Afterward, we tested the sensitivity of the fractal dimensions of crack patterns to the various parameters of the box-counting method. Finally, we investigated a

database of crack maps of brick masonry and concrete walls tested at EPFL [59,60] to determine the extent of the influence of each parameter and provide suggestions for the standardization of these parameters.

2. Key Definitions

2.1 Fractal Dimension

The goal of this paper is to determine the parameters required for calculating the fractal dimension (short: dimension) of a crack map, which is considered the "set" in our fractal studies. There are various methods for determining the dimension of a set, though the common point in all methods is that dimensions measure the set at various scales and investigate how these measurements change as the scale tends to zero [50]. For fractal geometries and approximately self-similar patterns such as crack patterns, this dimension is a fractional number between 1 and 2, which can be computed using the box-counting method explained in the following section.

2.2 The Box-Counting Method

A box-counting algorithm is a way of computing the fractal dimension of both exactly and approximately self-similar patterns [33,42]. For approximate (statistical) self-similar patterns, the fractal dimension is obtained over a given range of scales [41,42]. In the field of image processing, to investigate the dimension of binary patterns, i.e., black and white images, the pattern is covered by a set of grids with box sizes of r, and the number of boxes $N(r)$ that contain at least one black pixel is counted. The relation between r and $N(r)$ is defined as follows [42]:

$$N(r) = k \left(\frac{1}{r}\right)^{FD}, \tag{1}$$

where k is a constant, and FD is the fractal dimension. In practice, to compute the fractal dimension of a binary image, such as skeletonized crack patterns, these steps need to be followed:

1. **Creating a grid**: To create a grid, an arbitrary point (a) is assumed as the point where the grid is created, which is denoted as the *origin of the grid* [34,61]. In the following, it will be shown that the origin of the grid position and the orientation of the grid with regard to the crack pattern can influence the estimated fractal dimension.

2. **Placing the pattern on the grid**: In the second step, the bounding box, which is the smallest enclosing box that includes the pattern on the image [61,62], illustrated by the red box in **Fig. 2**, is defined. The minimum and maximum sizes of the wall and bounding box are w_{min}, w_{max} and b_{min}, b_{max}, respectively. Then, a fixed point of the bounding box, the bottom left corner in this example, is placed on the origin of the Cartesian coordinate system O. For illustration, these procedures are depicted in **Fig. 2**.
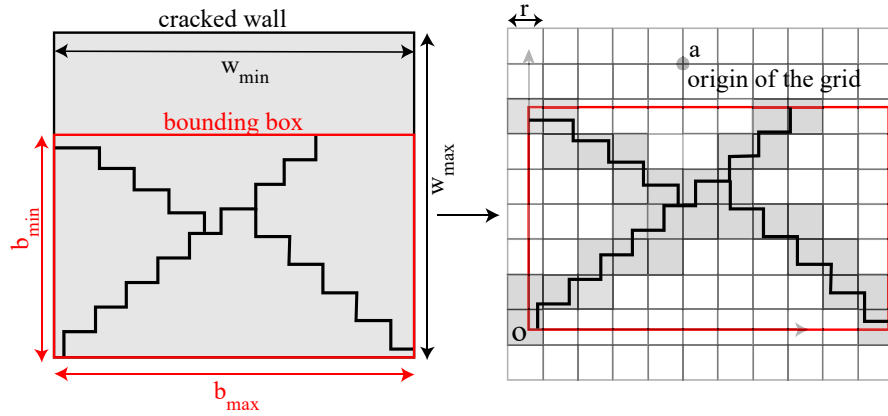
Fig. 2 Placing a bounding box on a grid with a box size of r.

3. **Finding the slope**: Grids of different sizes, for example, $r = 1, 2, 4, 8, \ldots, 2^n$ (scale factor of 2), are created according to step (1), and the number of boxes intersecting the object $N(r)$ is counted. To estimate the fractal dimension, $\log N(r)$ is plotted against $\log r$, and a line is fitted, typically using the least-squares method, to the points over the range where the points lie approximately on a straight line. The absolute value of the slope of the line is the estimation of fractal dimension, FD. **Fig. 3** illustrates the diagrams of $\log N(r)$ versus $\log r$ for two different cases. In **Fig. 3(a)**, the pattern can be delineated by reporting just one fractal dimension (FD_1) since there is only one scale interval ($r_1 < R1 < r_2$) wherein the plot is linear. However, the pattern in **Fig. 3(b)** is more complex, and two dimensions must be reported (FD_1 and FD_2) [29,62], because there are two intervals $r_1 < R1 < r_2$ and $r_3 < R2 < r_4$ wherein points fall on a straight line. As will be outlined later, one challenge is to determine over which range of scales the plot is approximately linear. In other words, the upper and lower limits of each interval, i.e. r_1, r_2, r_3, r_4, are referred to as cutoffs and must be determined. It has been shown that the choice of scale factor and the cutoffs influence the fractal dimensions of crack maps.
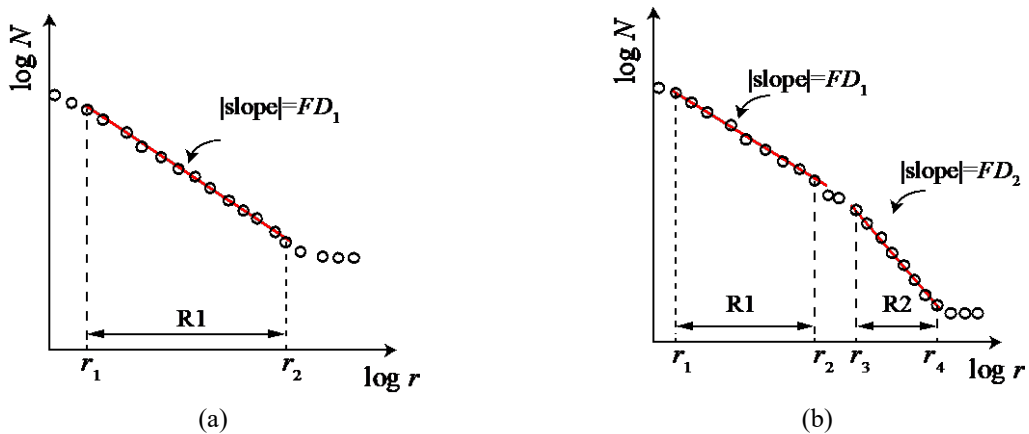

(a) (b)

Fig. 3 Plot of $\log N(r)$ versus $\log r$.
(a) Pattern with one *FD* and (b) pattern with two *FD*s.

With a deterministic monofractal, i.e., generated by a series of repetitive operations, a diagram like **Fig. 3(a)** is obtained, and the absolute slope will be the *estimation* of the fractal dimension that can also be calculated analytically. However, as alluded to earlier, the box-counting method can also be applied to patterns that are not deterministic fractals [33]. For crack maps, the fractal dimensions is obtained for the interval $r_3 < R2 < r_4$ in **Fig. 3(b)**, which is referred to as the fractal regime [44], are suitable for characterizing the complexity of crack patterns. The fractal dimension obtained for the interval $r_1 < R1 < r_2$ in **Fig. 3(a)** and **Fig. 3(b)** tends toward 1 if the crack pattern consists only of lines and not of patches (e.g. due to crushing of the material). Thus, it cannot describe the space-filling property of the crack patterns. In summary, **Fig. 4** shows different dimensions associated with different scale intervals [22,44]. In this figure, regions one and two are denoted as the Euclidean regime (where the fractal dimension is one at small scales) and fractal regime, respectively. R_E is the scale at which the behavior of the pattern changes from Euclidean to fractal and is associated with the spacing between the objects in an image [63]. R_F is the maximum size of the bounding box for which only one box is needed to intersect the pattern. Thus, the fractal dimension becomes zero in region three [22,44].
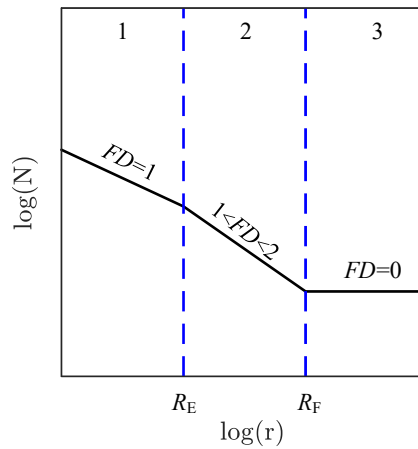

Fig. 4 Observed behavior of crack maps according to various scale intervals (adopted from [22,44]). Region 2 is a fractal regime, and regions 1 and 3 are non-fractal regimes. The range between R_E and R_F is the interval over which a fractal dimension can be defined.

By following these steps, it is possible to compute different *FD*s for the same image because some factors, like the position of the grid origin, the orientation of the grid, scale intervals, and scale factor, influence the results [31,32,34,51–58]. Moreover, other factors, like the thickness of the crack segments, can have a bearing on the estimated fractal dimension [64]. We will, therefore, show that it is necessary to report the estimate of a fractal dimension that is computed by the box-counting method together with the following information: 1) whether crack patterns were skeletonized or not; 2) grid position and orientation; 3) set of box sizes (or scale factor), and 4) box

size interval. Parametric studies on crack patterns of masonry and concrete walls provide recommendations for each factor to adjust the box-counting algorithm for obtaining the fractal dimension of crack patterns.

2.3 Set of example crack maps

The crack maps used as examples in this study have been obtained from three sets of experiments conducted at EPFL (**Fig. 5**) [49,59,60]. All three sets are quasi-static cyclic tests on walls:

a) Tests on large-scale brick masonry walls (PUP Series): Tests on six brick masonry walls (PUP1-6) with dimensions of 2010 mm × 2250 mm were carried out by applying different axial load ratios and shear spans, resulting in flexural, shear, and hybrid failure of the walls [59].

b) Tests on small-scale brick masonry walls (PUM Series): Tests on five brick masonry walls (PUM1-5) with dimensions of 1005 mm × 1113 mm were conducted to examine the influence of scaling masonry specimens on stiffness, strength, and failure mechanisms [60].

c) Tests on thin reinforced concrete walls (TW Series): Five thin reinforced concrete walls (TW) were tested to investigate the in-plane and out-of-plane behavior. Test units TW1-TW4 and TW2-TW3-TW5 measured 2620 mm × 2000 mm and 2580 mm × 2000 mm, respectively. The spacing of the horizontal reinforcement was 200 mm and 130 mm, respectively [49].

(a) (b) (c)

Fig. 5 (a) Test setup, (b) masonry walls [59,60], and (c) concrete walls [49].

Based on images taken during the tests (**Fig. 6**), skeletonized binary crack patterns were drawn in AutoCAD [65] at a scale of 1 pixel = 1 mm. In this study, 83 and 45 crack maps of masonry and concrete walls,

respectively, obtained at the maximum drift levels and zero forces were utilized. All of the images and results have been documented and are available online (https://eesd.epfl.ch/data_sets).
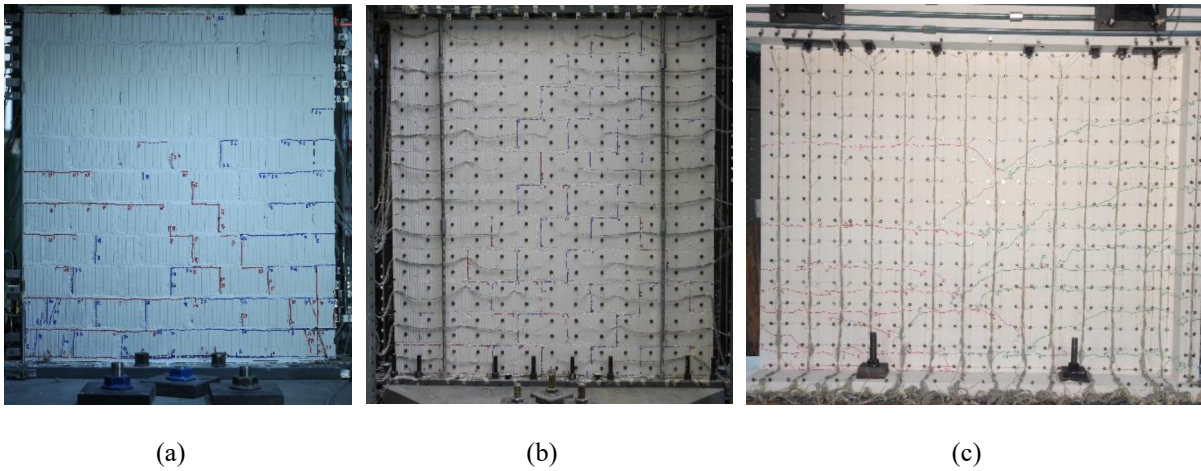

(a)   (b)   (c)

Fig. 6 Images that served as the basis for the crack maps. (a), (b) Masonry walls [59,60] and (c) concrete walls [49].

3. Fractal Dimension Sensitivity to Various Parameters

3.1 Grid Position and Orientation

Studying the various approaches regarding how to choose the grid position can be of critical importance; the origin of the grid position and orientation of the grid are effective factors for determining FD because they affect the number of boxes intersecting the pattern [31,51,53–55,64,66]. Some researchers (e.g. [55]) stated that to satisfy the boundary condition defined by Hausdorff [26], the minimum number of boxes intersecting the object should be determined for each box size. To do so, every possible position and orientation of the pattern must be examined at each scale, and the position in which the number of boxes is the smallest must be considered. In FracLac [61], a plugin for ImageJ [67] that is used for fractal analysis [33], however, a finite number of grid positions is randomly considered, and the value of FD at each grid position and orientation is computed. Gonzato et al. [64] suggested taking at least 20 random positions and reporting the average FD as the estimation of the fractal dimension. More recently, optimization techniques have also been used to find the rotation and location of the grid where the number of boxes intersecting the pattern reaches a minimum [31]. According to Falconer [50], there are two approaches for counting $N(r)$ for practical applications while the grid elements are rectangular: i) the number of boxes intersecting the pattern, and ii) the minimum number of boxes that cover the pattern. In the former method, there is no need to find the minimum number of boxes. In the latter, however, at each scale (r), the position and orientation of the grid at which the number of boxes intersecting the pattern is minimalized must be determined.

8

To show the effect of grid orientation and position of the origin of the grid, an image on which there is a diagonal line is examined in **Fig. 7**. In the initial configuration (**Fig. 7(a)**, eight boxes are intersected. By changing the position of the origin of the grid in **Fig. 7(b)** and rotating the grid in **Fig. 7(c)**, the number of intersected boxes changes to seven. Therefore, these two factors influence the number of intersected boxes.
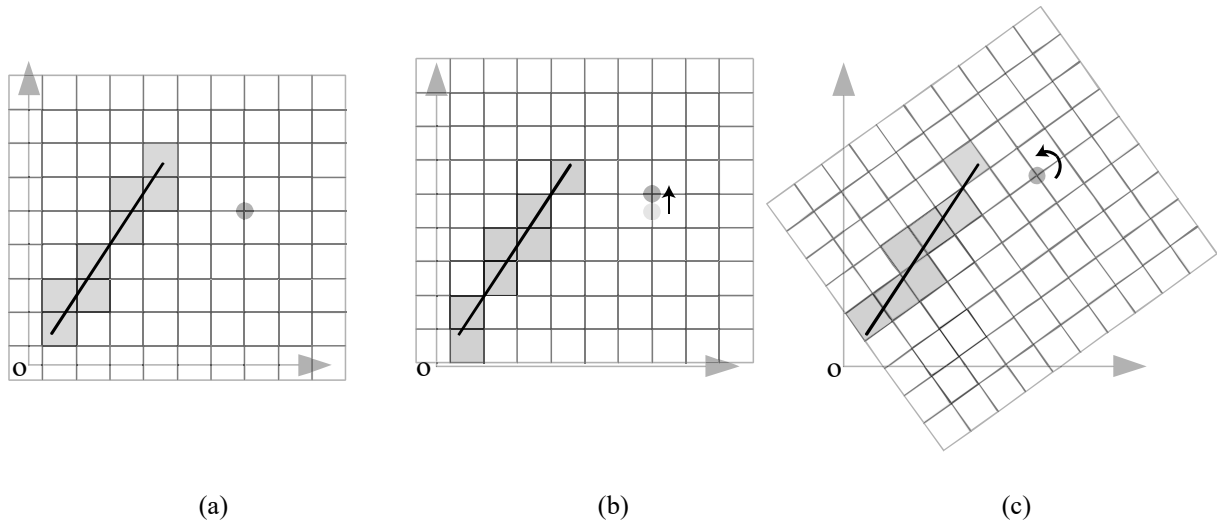

(a)   (b)   (c)

Fig. 7 Illustration of the influence of the origin of the grid position and the orientation of the grid. (a) Initial position, $N = 8$; (b) changing the position of the grid, $N = 7$; and (c) changing the orientation of the grid, $N = 7$.

For crack maps, as the size of the bounding box is not necessarily a multiple of the scale, the position of the origin of the grid can also influence the *FD*. To investigate this effect, the origin of the grid has been considered as the bottom right corner, bottom left corner, top right corner, and top left corner of the bounding box, and the orientation of the grid is assumed to be parallel to the sides of the wall. **Fig. 8** shows the difference between the maximum and minimum of the computed *FD*s for the crack patterns contained in the concrete and masonry databases that have a fractal behavior. Among the available crack maps, 61/83 for masonry walls and 30/45 for concrete walls show fractal behavior, i.e., the slope of the interval $r_3 < R2 < r_4$ in **Fig. 3(b)** is greater than 1.0. It can be observed that the choice of the origin of the grid location can change the fractal dimension up to 0.5. **Fig. 8** shows that the effect was stronger for masonry walls than for concrete walls.
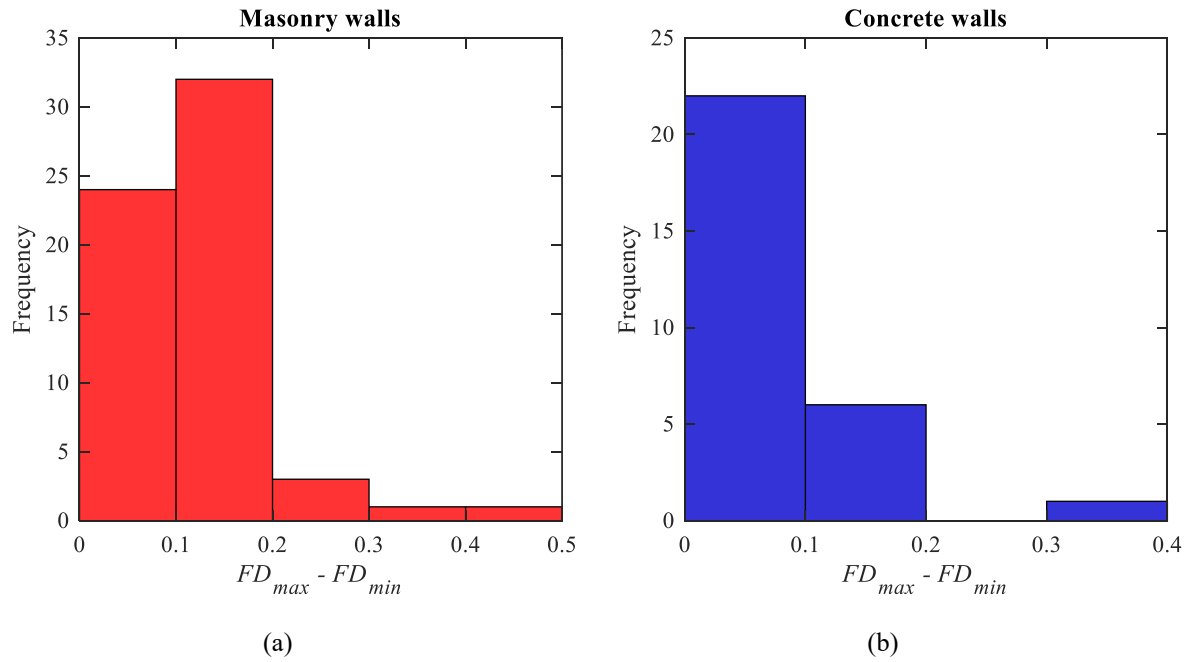
Fig. 8 Influence of the grid position (without rotation) on the obtained *FD*.
(a) Masonry walls, wherein 61/83 showed fractality [59,60], and (b) concrete walls, wherein 30/45 showed fractality [49].

Besides taking the four corners, choosing a random point inside the bounding box as the origin of the grid is possible, and based on the obtained results in the previous analysis, it is expected to change the *FD*. To tackle this issue, one solution is that researchers must report at least the origin of the grid position and grid orientation—its influence is addressed at the end of this section—in any studies establishing correlations between estimated fractal dimensions and some physical properties. Another solution involves calculating the mean value of the fractal dimension by considering multiple random positions [61]. **Fig. 9** illustrates the change in the mean value of *FD*s due to considering 1, 5, 10, 15, 20, 25, and 30 random positions inside the bounding box (the mean is normalized by the value obtained at 30 random positions). It is observed that for both databases, the mean values of fractal dimensions steady at around 25 random positions. The final possible solution is to find the minimum number of boxes intersecting the cracks, which requires exhaustive search or optimization procedures. Unfortunately, in most of the papers conducting the fractal analysis of crack patterns on walls, the origin of the grid position has not been mentioned, making their results not reproducible.
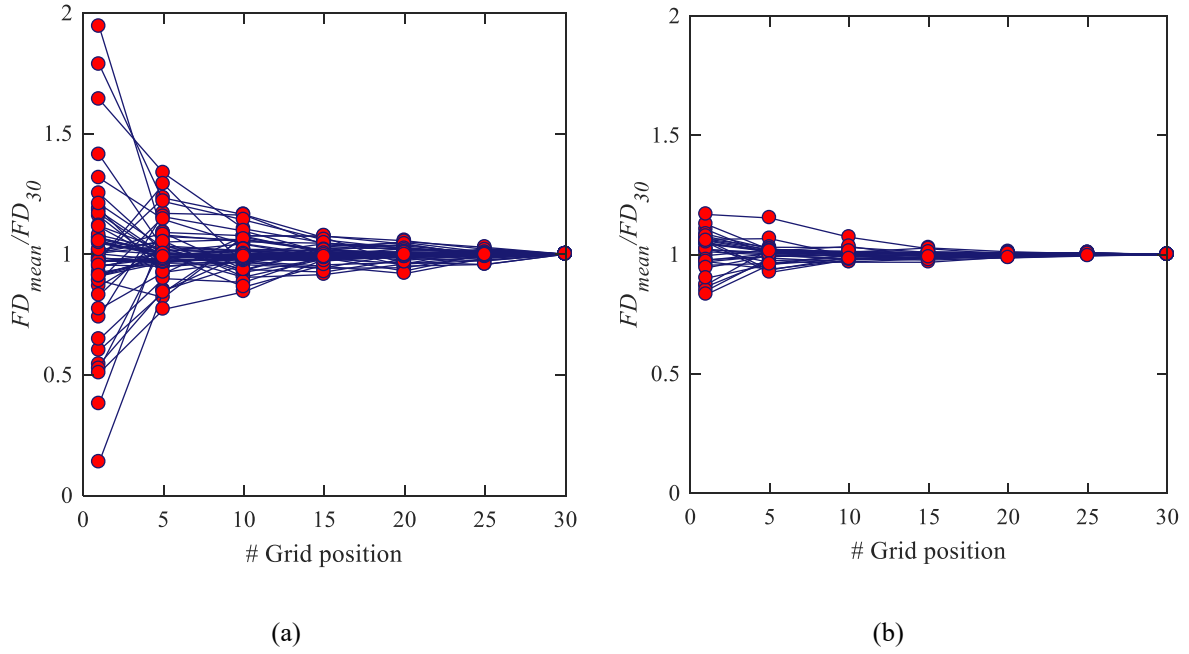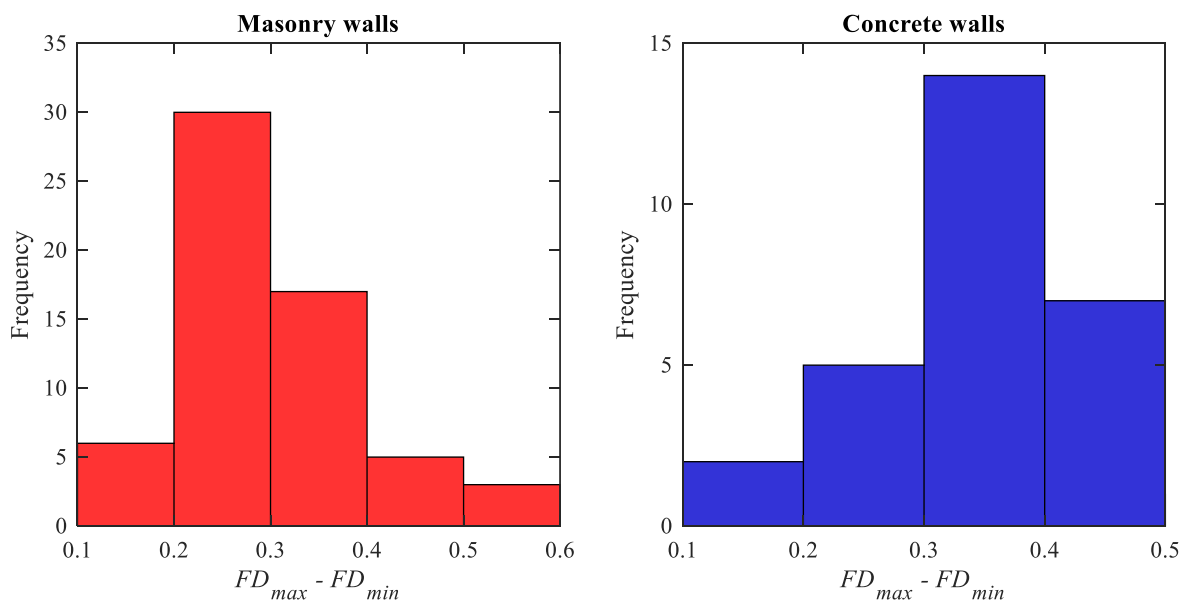
(a)   (b)

Fig. 9 Mean *FD*s calculated using a # of random grid positions as specified on the X-axis (a) Masonry walls

[59,60] and (b) concrete walls [49].

To explore the impact of grid rotation on the estimation of fractal dimension, the bounding boxes encompassing the crack patterns were rotated with respect to the horizontal axis with angles ranging from $0°$ to $180°$ (with the step of $10°$). From **Fig. 10**, it can be concluded that whereas the maximum range in the masonry database is greater than in the concrete database, this factor is more influential for the concrete crack maps since the computed range is around 0.4 for more than half of the database. This can be due to the higher randomness in the crack spacing of concrete walls compared to the masonry walls where the crack spacing of multiples of one brick height dominate.

Fig. 10 Influence of the grid rotation on *FD*.
(a) Masonry walls, wherein 61/83 show fractality [59,60], and (b) concrete walls, wherein 30/45 show fractality [49].

3.2 Scale Factor for Box Sizes

Several studies have been conducted to find the influence of the various sampling strategies (e.g. [34,56]) on the computation of the estimated fractal dimension by the box-counting method. It was determined that white areas around the pattern affect the results [34]. In general, any white spaces added to the pattern during the covering procedure might lower the accuracy of the box-counting method [42]. Additionally, a sequence of discrete box sizes, typically multiples of a basic box size, must be chosen [34], and enough box sizes must be considered to fit the straight line, as shown in **Fig. 3** [56]. Often, a scale factor of 2 is chosen, and the powers of 2 ($r = 1, 2, 4, 8, \ldots, 2^n$) are taken as the set of sampling sizes [29]. This approach has also been used in previous studies addressing the fractal dimensions of crack patterns [21,22,44]. However, it is not always the best sampling strategy, especially if the given image has dimensions that are not powers of 2 [52].

The relative size of the bounding box and the size of the elements of the pattern can assist in the choice of an appropriate scale factor. For example, **Fig. 11(b,c)** demonstrates the impact of the scale factor for the box sizes on the estimated value of the fractal dimension of the *box fractal* (**Fig. 11 (a)**), whose exact fractal dimension is 1.4647. The smallest elements in this binary image are 3×3 filled squares with the dimension of 81×81 pixels. According to the **Fig. 11(b)**, the *FD* is close to the exact fractal dimension when the scale ratio is three and the set of box sizes r = 1, 3^1, 3^2, 3^3, 3^4. However, if a scale factor of 2 is used and the set of box sizes is r = 1, 2^1, 2^2, 2^3, 2^4, 2^5, 2^6, the obtained *FD* is lower than the true fractal dimension (**Fig. 11 (c)**). As demonstrated in **Fig. 13**, this difference in the scale factor can affect the results (up to 0.5 difference in the estimation of *FD*); in the example, the difference in computed *FD* is, however, relatively small (2.9%).
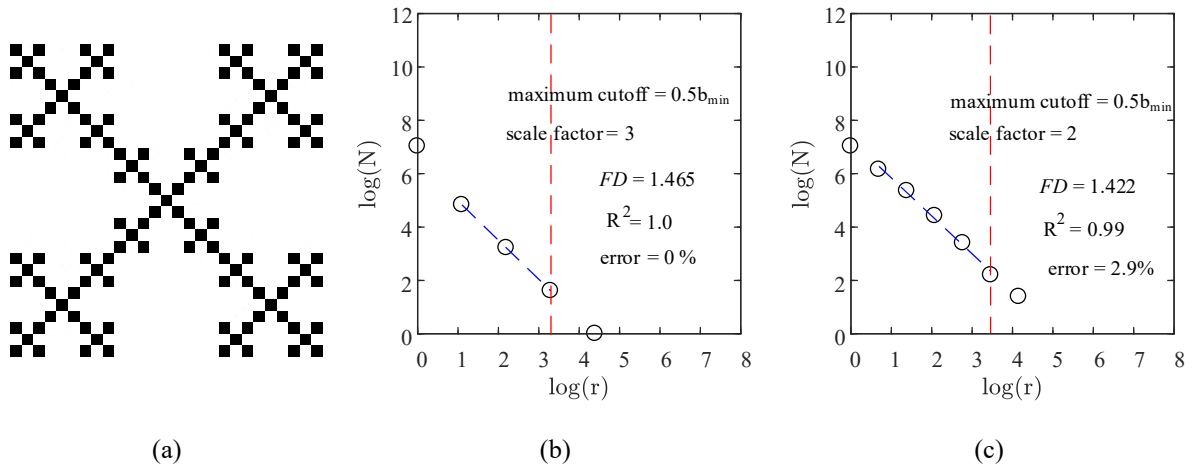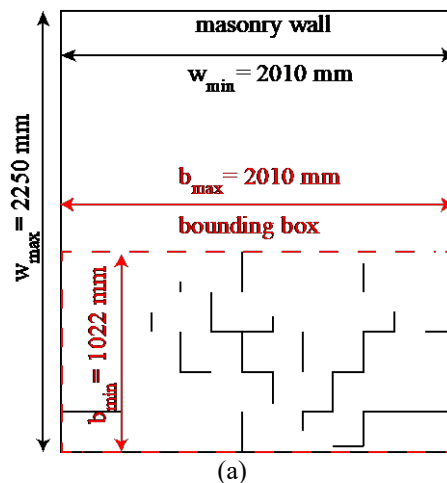

(a)   (b)   (c)

Fig. 11 Influence of the scale factor on estimating the fractal dimension of the (a) "box fractal" (image adopted from [42]). Scale factor of (b) 3 and (c) 2.

Along with the scale factor, there have been some suggestions for how to include the appropriate number of points to fit the linear line to reduce errors [34,68]. To test this, a wide range of scale factors, including 1.1, 1.2, 1.3, 1.4142 ($\sim\sqrt{2}$) … 2, has been assumed to evaluate the effect of scale factor on the estimation of fractal dimensions [34]. Among these scale factors, the square root of 2 is advised by some authors [34,64]. In another more recent attempt, So et al. [52] developed a new sampling method in which the number of boxes intercepted by the black pixels could be a non-integer number as opposed to the conventional box-counting algorithm. By considering non-integer box numbers, the estimation of fractal dimensions was more precise for fractal geometries.

For non-mathematically fractal structures such as crack maps, however, there is no benchmark with which to compare the results of the computed *FD*. In these cases, by implication, it is advisable to assume a scale factor that provides more points that deviate only minimally from the line for the linear fitting, since insufficient sampling sizes and narrow intervals might lead to anomalous results [52,69]. **Fig. 12** compares the results obtained by assuming two different scale factors for one of the crack maps in the masonry database. It is evident that with the scale factor 2, there are only two points in the fractal region that can be used to fit the line, which is not suitable, whereas the scale factor $\sqrt{2}$ gives three points to fit the line. **Fig. 13** shows the distribution of the range of *FD*s for different scale factors, including 1.1, $\sqrt{2}$, 1.6, and 2. It is evident that for both masonry and concrete crack patterns, changing the scale factor could change the *FD* up to 0.5, which shows the high sensitivity of *FD* to this factor.
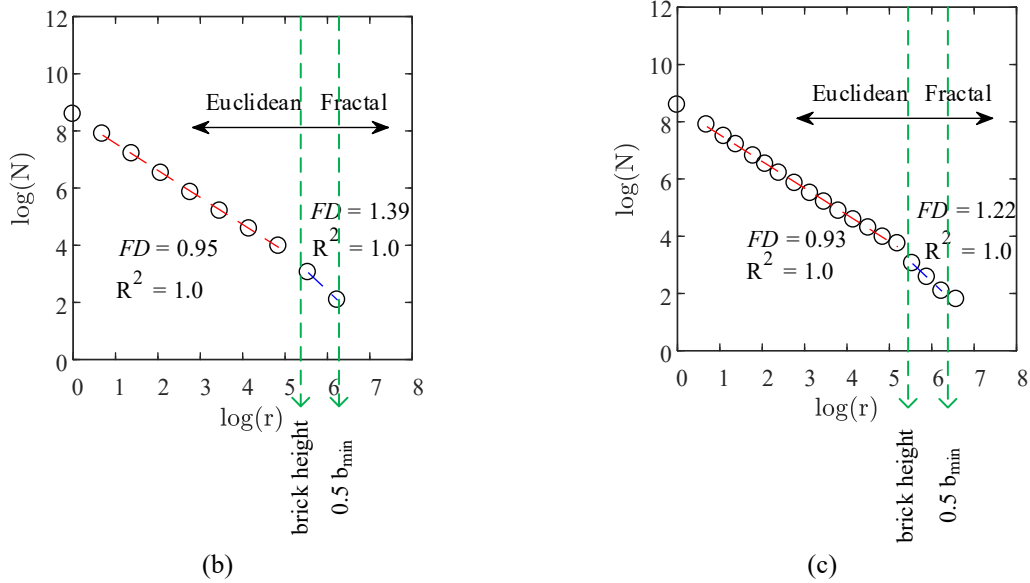

(a)

Fig. 12 Comparison of the scale factors (b) 2 and (c) $\sqrt{2}$ on the *FD* of a crack map (a) of the masonry wall PUP6 at a drift level of 0.10% [59]. As can be seen from the blue-fitted line, the scale factor of 2 only provides two points to fit the line, whereas a scale factor of square root 2 provides three.
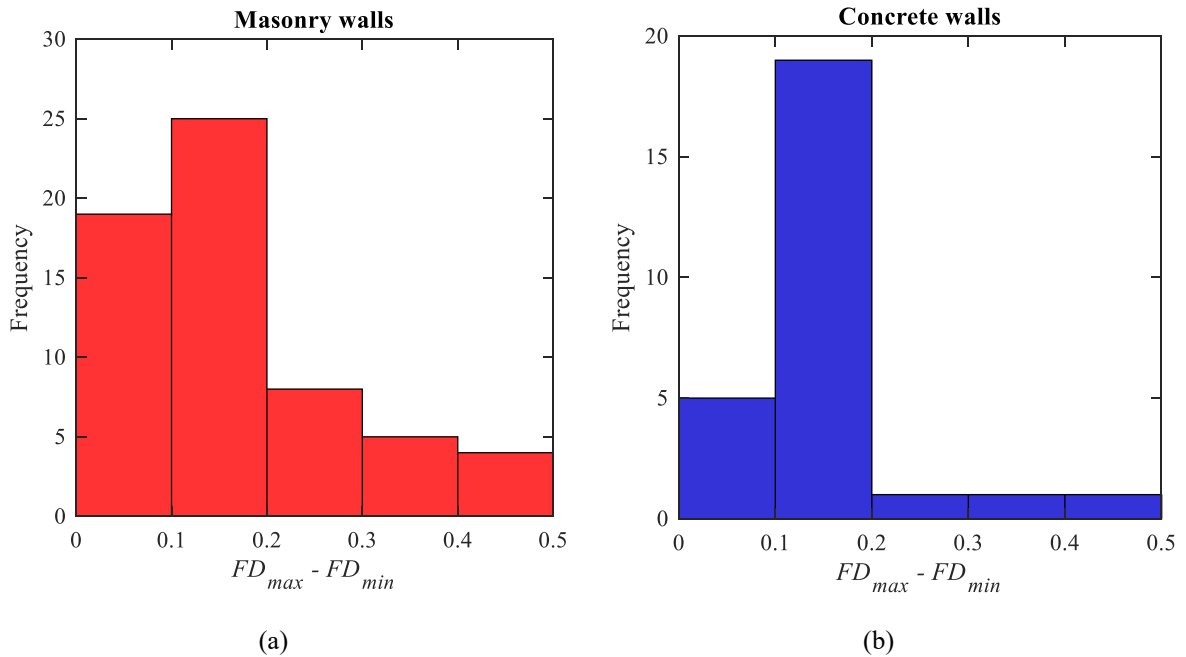

Fig. 13 Influence of scale factor on *FD*.
(a) Masonry walls, wherein 61/83 show fractality [59,60], and (b) concrete walls, wherein 30/45 show fractality [49]. The high differences between the FD_{max} and FD_{min} show the sensitivity of estimating *FD* to the choice of the scale factor.

3.3 Box size Interval

Calculating the fractal dimension of crack maps can be affected by the box size interval, which is the interval over which a self-similarity of the crack pattern is assumed, i.e., the range of scales over which $\log N(r)$ - $\log(r)$ graphs, such as those shown in **Fig. 3**, are assumed as linear. Complex patterns often cannot be described by reporting just one dimension for the whole range of scales. Therefore, for each range of scales that follows a linear trend, the corresponding dimension must be determined as shown in **Fig. 4**. For crack maps of unreinforced

14

masonry and reinforced concrete walls, we have observed patterns that can be described either by one or by two fractal dimensions (**Fig. 3(a)** or **Fig. 3(b)**). In general, when there are a few unconnected cracks like **Fig. 17**, the results will be like **Fig. 3(a)**; alternately, as the cracks grow and spread over the whole wall, the graph will be similar to **Fig. 3(b)**. In the following, some suggestions are made for choosing the global minimum cutoff r_1 in **Fig. 3**, the global maximum cutoff r_2 in **Fig. 3(a)** and r_4 in **Fig. 3(b)**, and the location of breakpoint r_2 or r_3 in **Fig. 3(b)** when determining the fractal dimensions of crack maps. In practice, the scales r_2 and r_3 can also be assumed to be equal. Further details about this assumption are explained in section 3.4.

For the value of the global maximum cutoff, some studies have used 25% of the shorter side of the bounding box (b_{min}) [34,70,71]. Harrar and Hamami [57] used twice this global maximum cutoff (0.5 b_{min}) to calculate the fractal dimension of gray-scale images. Roy et al. [55] also considered 0.5 b_{min} when computing fractal dimensions of fracture systems. For the global minimum cutoff, Foroutan-pour et al. [53] proposed a range of one to five pixels. They expressed that the best minimum size is the point, after which there is a deviation from the fitted straight line and verified their suggestions by analyzing some well-known fractal geometries. Koch [70] proposed that 0.03 b_{min} should be considered as the global minimum cutoff [34]. Roy et al. [55] suggested plotting the standard deviation of the slope of the fitted line versus box sizes, wherein the minimum cutoff would be where the graph constantly remains at zero.

Specifically for crack maps, Farhidzadeh et al. [22] assumed the maximum cutoff based on the maximum crack length, and for the minimum cutoff, they considered the point where the fractal changes to the Euclidean regime. Dolatshahi and Beyer [44] used the wall size as the global maximum for finding the structural fractal dimension of crack patterns on masonry walls because the cyclic loads caused the cracks to spread over the whole wall. Carrillo and Avila [38] used the software *Benoit* [72] to compute the fractal dimensions of cracks on concrete walls. In most of the studies in this field, the effect of the global maximum cutoff, which is determined by the size of the bounding box, was not investigated. Table 1 summarizes different maximum and minimum cutoffs that have been used in different articles.

Table 1. Maximum and minimum cutoffs proposed for non-mathematical fractal patterns in literature.

Reference	Minimum cutoff	Maximum cutoff
Ostwald [34], Cooper and Oskrochi [71]	0.03 b_{min}	0.25 b_{min}
Roy et al. [55]	Using the derivative of the standard deviation of *FD*	0.5 b_{min}
FracLac plugin for ImageJ software [61]	Variable	0.2-0.5 b_{min}

Foroutan-pour et al. [53]	One to five pixels	0.25 b_{min}
Farhidzadeh et al. [22]	Change of fractal to Euclidean	Maximum size of the object (crack)
Dolatshahi and Beyer [44]	One pixel	Wall size

3.4 Breakpoint Location

For some patterns, such as the crack maps depicted in **Fig. 14**, there is an apparent slope change in the log-log plots (**Fig. 3[b]**), meaning two fractal dimensions must be reported to characterize the complexity. As long as the value of the coefficient of determination is high, it is feasible to assume one breakpoint location, i.e., $r_2 = r_3$ in **Fig. 3(b)**. To determine the fractal dimension of crack patterns, the location of the breakpoint and the global minimum and maximum cutoffs must be defined. It is shown that the breakpoint of crack maps is related to the crack spacing (also reported in previous studies like [44]). In brick masonry walls, the crack spacing is very regular because it is determined by the brick size [44]. In concrete walls, it is somewhat less regular. For this reason, the breakpoint location for masonry and concrete crack maps is investigated separately.

When crack patterns in the masonry database showed apparent fractality over a range of scales, two different plots representative of a portion of the database were obtained, as depicted in **Fig. 14**. In both types of crack maps, the fractal dimension is 1 in the first part of the graph, meaning that the pattern does not show fractality in this range. In the second part, however, the pattern shows fractal behavior, and *FD* is a fractional number between 1 and 2. The location of the breakpoint relates to the vertical/horizontal distances between cracks [44]. For brick masonry walls, it was postulated [44] that the breakpoint location is roughly equal to the smaller dimension of the bricks [44]. In fact, as bricks have a uniform size and cracks mainly follow joints, the crack spacing in these walls is approximately uniform [44]. In **Fig. 14**, the black, blue, and red dashed lines highlight the location of the breakpoint, 0.5 b_{min}, and b_{min}, respectively. In some crack patterns, all points after the breakpoint fall on the same line, as shown in **Fig. 14(a)**. However, an arrow at the last point in a graph in **Fig. 14(b)** indicates it does not follow the fitted line and should therefore not be considered. It should be pointed out that all analyses in this section have been conducted with the following assumptions: the origin of the grid is the left bottom corner of the bounding box, the orientation of the grid is considered to be parallel to the wall sides, and the scale factor is presumed to be $\sqrt{2}$, i.e., $r = 1, \sqrt{2}, \sqrt{2}^2, \dots, \sqrt{2}^n$.
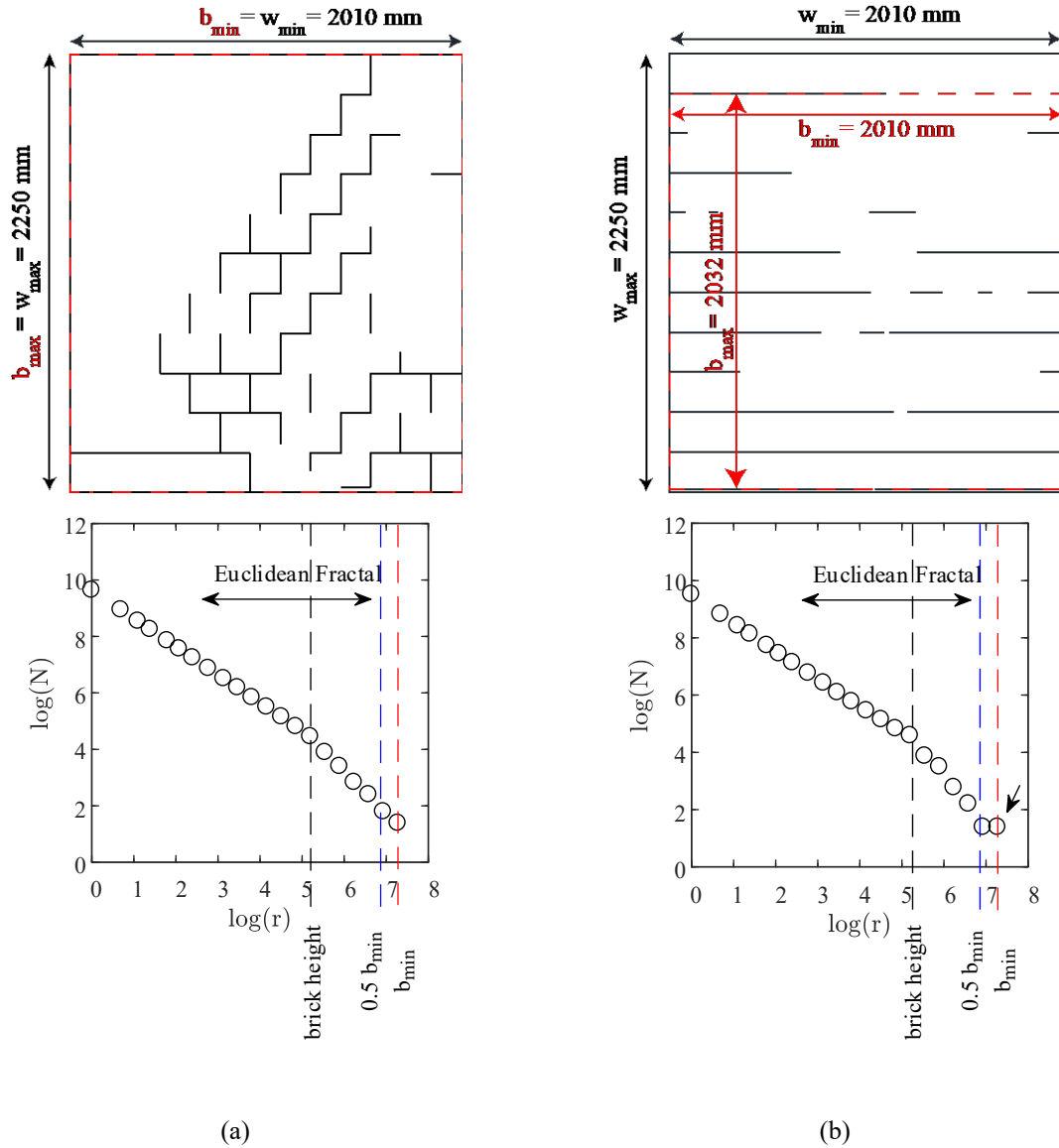
<table>
<tr><td>(a)</td><td>(b)</td></tr>
</table>

Fig. 14 Box size interval and the breakpoint location for walls in the masonry database [59,60]. (a) Crack map of the brick masonry wall PUP6 at a drift level of 0.15%, and (b) crack map of the brick masonry wall PUP3 at a drift level of 0.30%.

To demonstrate the difference that the global maximum cutoff can make on the calculations, **Fig. 15(a)** compares the histograms of *FD* computed under two assumptions for the global maximum cutoff: $0.5 \, b_{min}$ and b_{min}. This analysis was conducted only for the crack patterns that have a fractal regime in their plot, like **Fig. 3(b)**; there are 83 crack maps in the masonry database, of which 61 show statistical fractality. The other 22 crack maps contain too few cracks for a fractal dimension to be defined (see discussion at the end of this section). It is evident that in both cases, the value of the coefficient of determination is high (**Fig. 15(b)**), although the results can be quite different (**Fig. 15(a)**). Indeed, the differences between the maximum and minimum *FD*s are around 0.2 (**Fig. 15(c)**). Moreover, the mean of the distribution, as demonstrated in **Fig. 16**, is 1.00, which means that the choice of

the current breakpoint location and the choice to consider the global minimum to be greater than one pixel—i.e., excluding the first point where $r = 1$—are appropriate assumptions.
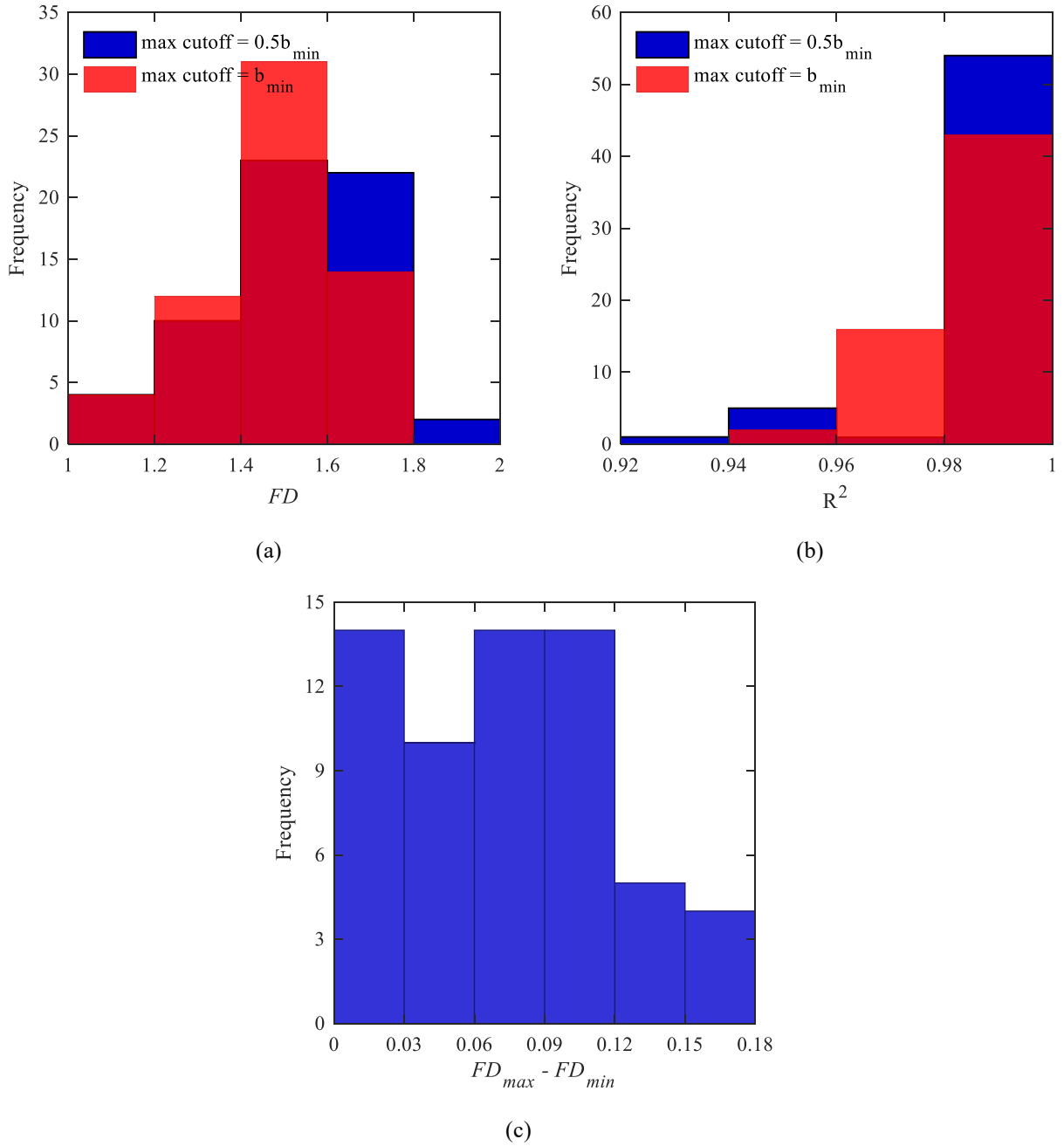

(a)

(b)

(c)

Fig. 15 For brick masonry walls, the influence of global maximum cutoff on (a) FD of masonry database and (b) the coefficient of determination. (c) The distribution of the difference between FD computed with a maximum cutoff of 0.5 b_{min} and FD computed with a maximum cutoff of b_{min}.
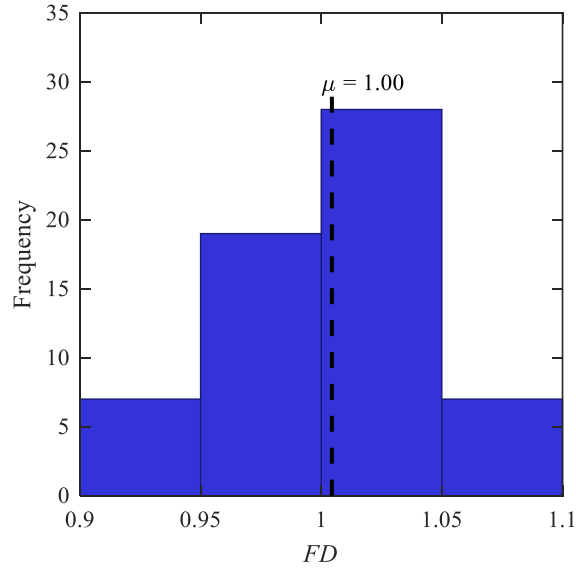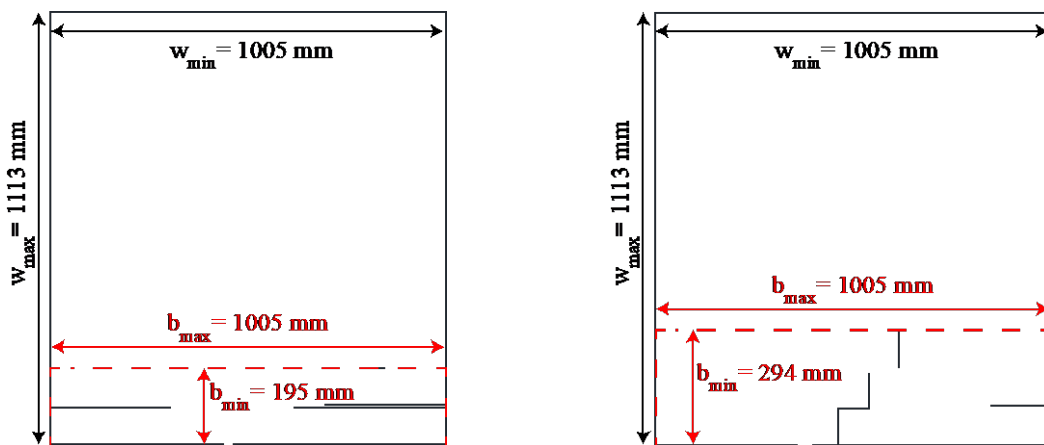
Fig. 16 Histogram showing the distribution of *FD* in the Euclidean regime for walls in the masonry database [59,60].(This result obtained by setting the global minimum to $r = 1$ and the breakpoint location to the height of the brick.)

As mentioned previously, **Fig. 15** represents only 61/83 crack patterns within the masonry database. If the crack maps contain only a few cracks, no fractal behavior can be observed, and these patterns were therefore not included in the analysis of **Fig. 15**. Two examples of the 22 images of crack maps not showing fractality and their corresponding $\log N(r)$ - $\log(r)$ plot are shown in **Fig. 17**. In these plots, there is only one linear trend in the graph (like **Fig. 3(a)**) related to the Euclidean dimension, which is not capable of representing the complexity of the crack patterns. In these cases, other fractal dimensions, like an extended fractal dimension that captures the visual complexity of a pattern, could be more useful [39,73].
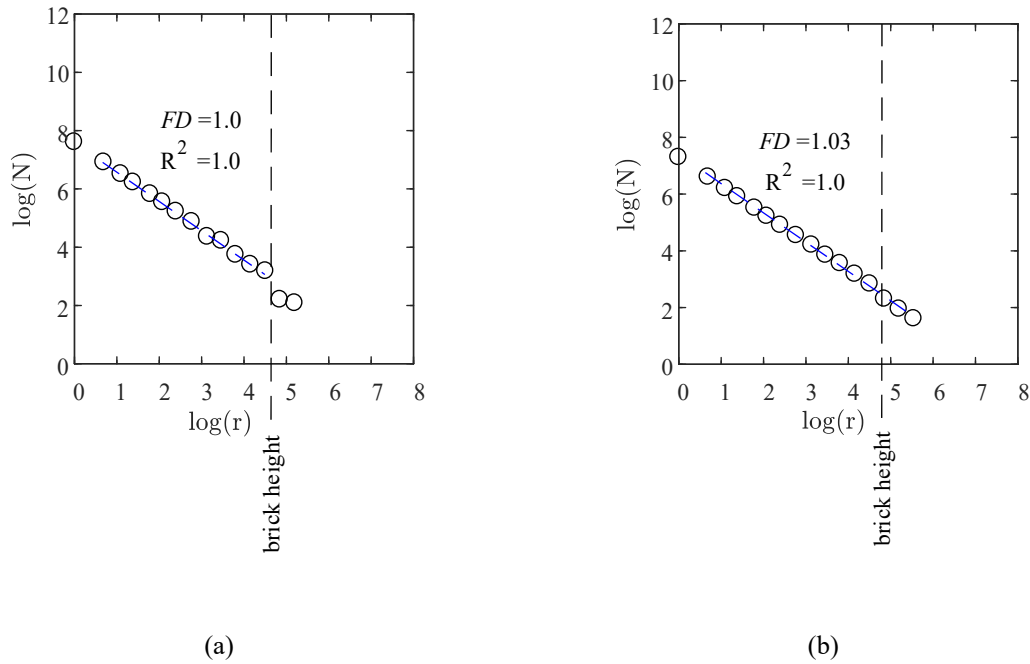
Fig. 17 Examples of crack maps lacking fractality [60]. (a) Crack map of the masonry wall PUM4 at the drift level of 0.20%. (b) Crack map of the masonry wall PUM5 at the drift level of 0.15%.

To account for the less-regular crack patterns in concrete walls, the effects of cutoffs on their calculated fractal dimension are now addressed. Like crack maps in brick masonry walls, the global maximum cutoff for crack patterns showing fractal behavior in concrete walls can either be 0.5 b_{min} or b_{min} (**Fig. 18**). Thus, the maximum cutoff can be determined according to the number of points that fit the straight line and the value of the coefficient of determination. Moreover, **Fig. 18** represents only a group of crack maps in the concrete database due to unconnected cracks that lack fractal behavior in several of the walls. Out of 45 crack patterns in the concrete database, 30 maps show statistical fractal behavior.

Because the crack spacing is not as uniform in concrete walls as in brick masonry walls, determining the breakpoint location is more difficult for concrete. As mentioned previously, the breakpoint location pertains to the crack distance. In concrete walls, the horizontal crack spacing is often controlled by the spacing of the horizontal reinforcement. For this reason, the smallest crack spacing typically occurs in the boundary elements where the spacing of the horizontal reinforcement is smaller than in the web, i.e., in between the boundary elements. Investigating the plots obtained for the crack maps showing fractality, the point where the regime changes is mostly associated with the spacing of transverse reinforcements. This can be verified by investigating the histograms that show the frequency of the crack distances (vertically). It can be observed that most of the crack distances are lower than 200 mm and 130 mm—the values corresponding to the spacing of the transverse reinforcements—for the crack maps in **Fig. 18(a)** and **Fig. 18(b)**, respectively.
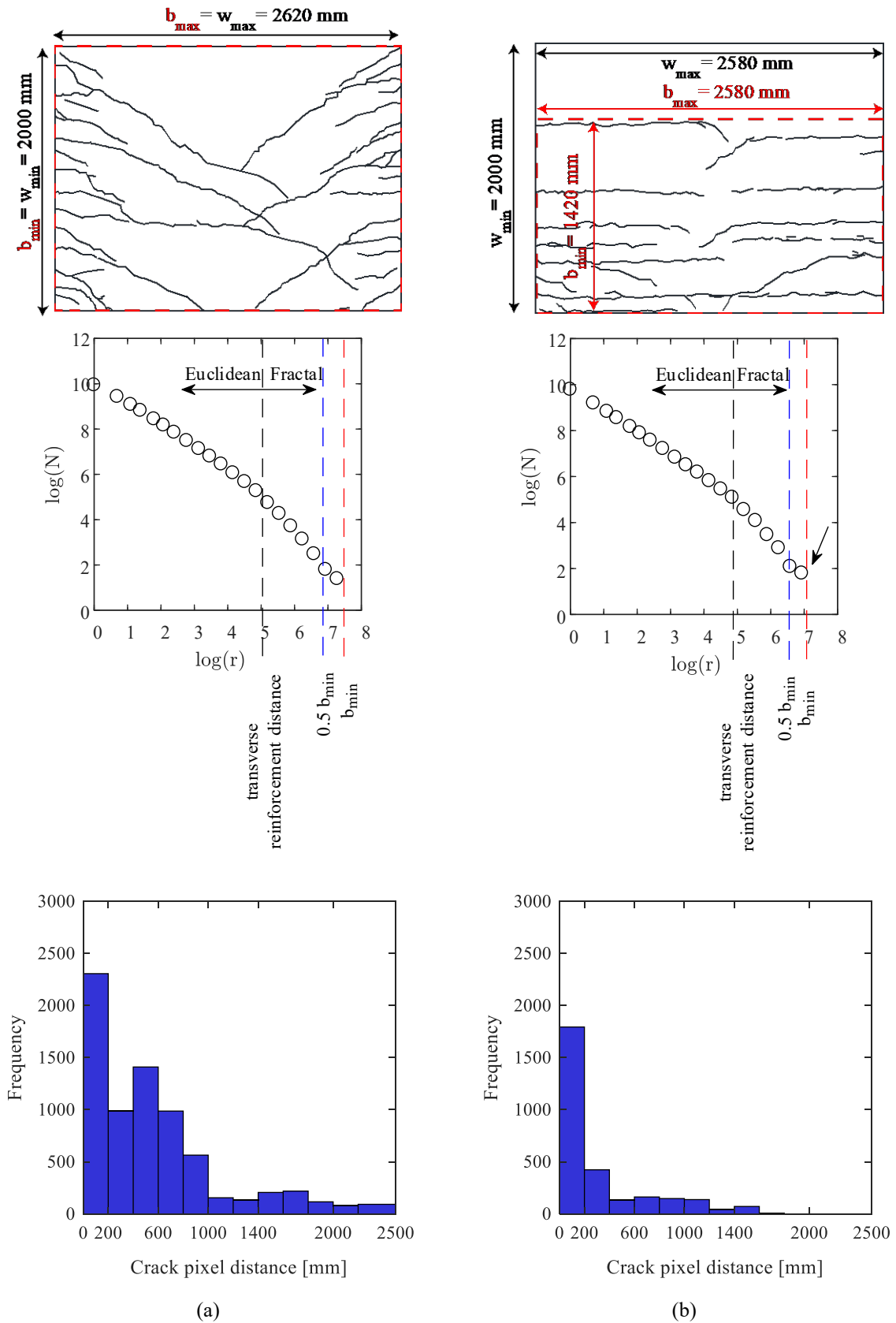
20

Fig. 18 Box size interval and breakpoint location for the walls in the concrete database [49]. (a) Crack map of the concrete wall TW1 at a drift level of 0.25%. (b) Crack map of the concrete wall TW5 at a drift level of 0.12%.
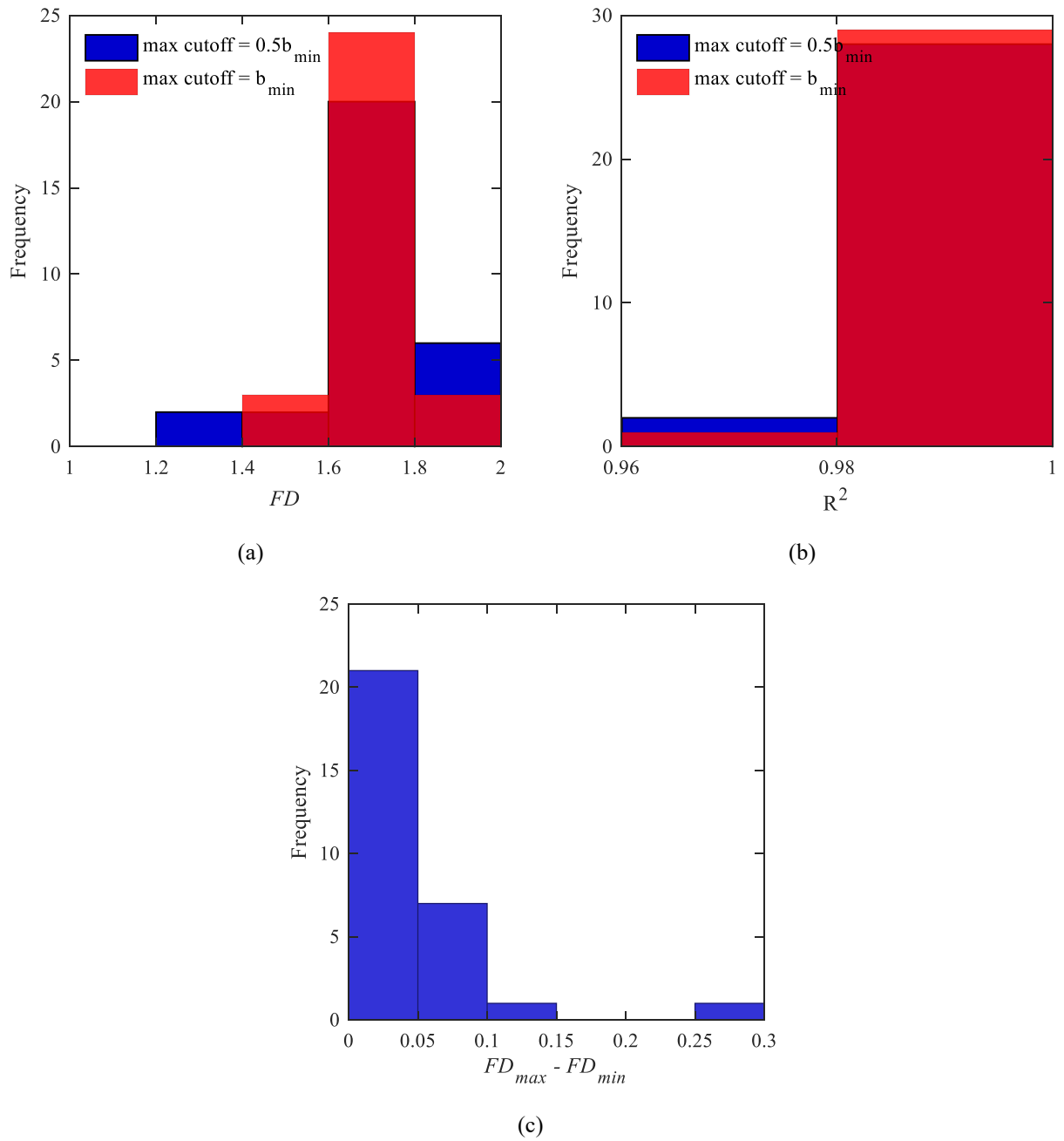
(a)

(b)

(c)

Fig. 19 For concrete walls, the influence of global maximum cutoff on (a) the *FD* of walls in the concrete database [49] and (b) the coefficient of determination. (c) The distribution of the difference between *FD* computed with a maximum cutoff of 0.5 b_{min} and *FD* computed with a maximum cutoff of b_{min}.

From **Fig. 19(c)**, it can be deduced that, for most cases, the estimated fractal dimensions of concrete crack

patterns are not hugely affected by the choice of the maximum cutoff. In the masonry database, the ranges (**Fig.**

15[c]) were more variable and, on average greater than those of concrete crack maps, meaning that the estimated

fractal dimension of the masonry crack patterns is more sensitive to the global maximum cutoff. As depicted in **Fig. 20**, the mean value of the Euclidean *FD* is 1.04, which is quite close to 1.
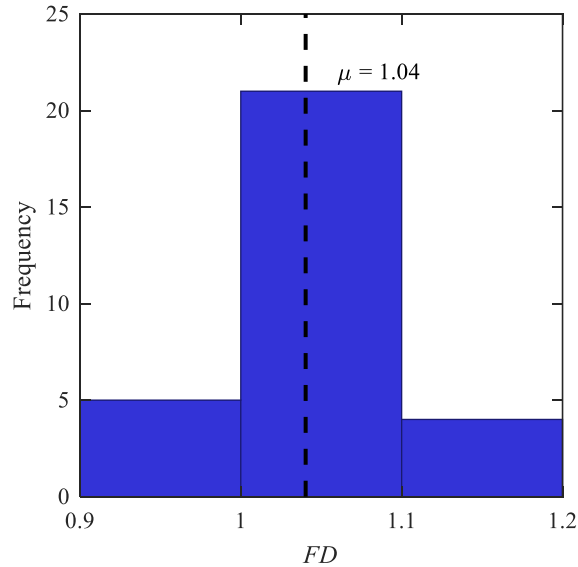

Fig. 20 Histogram showing the distribution of *FD* in the Euclidean regime for walls in the concrete database [49].

4. Conclusions

In this study, the box-counting method that is generally used to estimate the fractal dimension of both deterministic and non-deterministic fractals is reviewed. Various parameters affecting the results, including sampling sizes, maximum and minimum cutoffs, grid position and orientation, and breakpoint location are investigated. For each of these factors, suggestions provided by previous studies, which have been obtained mostly by exploring mathematical fractal geometries, are indicated. Furthermore, some new recommendations for exploring the fractality of crack maps are introduced by analyzing two databases containing 45 and 83 crack maps from concrete and masonry wall surfaces, respectively, that were tested at EPFL [49,59,60]. The results from these investigations are summarized in the following.

Box size interval: The box size interval is the interval over which a self-similarity of the crack pattern is assumed, i.e., the range of scales over which $\log N(r)$ - $\log(r)$ graphs are assumed as linear. To determine the maximum size of the interval, the results when taking 0.5 b_{min} and b_{min} as the maximum limit were compared. Based on the obtained high values for the coefficient of determination, it was shown that both values can be used as the global maximum cutoff. It should be pointed out that for a group of crack maps, however, one must consider 0.5 b_{min}, since the points after this limit might not fall on the same line as others.

Breakpoint location: For some crack maps, there is an apparent slope change in the log-log plots, meaning two fractal dimensions must be reported to characterize the complexity. Because only the part of the $\log N\,(r)$ versus $\log r$ plot indicating fractal behavior is of concern, one must define the location where the behavior of the crack maps changes from Euclidean regime to fractal regime. This point pertains to the crack spacing. The crack spacing in brick masonry walls is almost uniform because the cracks mainly pass through the joints, so the brick height can be considered as the breakpoint location. For concrete crack maps, the distance of the transverse reinforcement is suggested as the breakpoint location. It is important to point out that in both crack map databases, a portion of the patterns does not show any fractal behavior (*FD*=1), so other dimensions like extended-box counting could be used for evaluating the visual complexity of these patterns [39,73].

Sampling strategy: The sampling strategy refers to the sequence of discrete box sizes r, for which N is evaluated. Typically multiples of a basic box size are chosen, and the ratio of two consecutive box sizes is referred to as scale factor. The considered scale factor for the box sizes should provide enough points, at least three, that can be used to fit the line. For the examined crack map databases, the scale factor of $\sqrt{2}$ was the best, as was also suggested by previous studies concerning fractal geometries [34,64]. The box sizes should, therefore, be $1, \sqrt{2}^{1}, \sqrt{2}^{2}, \sqrt{2}^{3}, \ldots, \sqrt{2}^{n}$.

Grid disposition and orientation: The origin of the grid position and orientation of the grid with regard to the wall edges affect the computed *FD*. Based on the considerable differences that can be measured by changing the variables involved in the box-counting method, the origin of the grid position and the orientation of the grid must be reported for each analysis to make the results comparable. Moreover, it is possible to either choose different grid positions and orientations and take the mean value of the computed fractal dimensions or to find the optimum grid configuration, which is considered as the grid position that leads to the lowest *FD* [31,61,64].

In summary, non-deterministic fractal patterns, like crack maps, do not have a benchmark with which to compare the results of the estimated fractal dimensions. Therefore, it is of the upmost concern that any parameters used in the analysis are clearly defined. In this study, general suggestions are provided to aid in the choice of the scale factor, grid position and orientation, breakpoint location, and the cutoffs. For the crack maps of brick masonry and concrete walls that were investigated here, it was shown that the fractal dimension computed by means of the box-counting method is particularly sensitive to assumptions with regard to the grid orientation and the scale factor. The computed fractal dimensions were less sensitive for the grid position with regard to the wall edges and the global cut-off, i.e., the maximum box size considered. However, further studies addressing databases containing

more crack patterns are needed to deeply investigate the influence of each parameter on the fractal dimension of crack patterns. This study also showed that crack maps have only fractality if the crack map contains a certain number of cracks. If the crack maps contain too few cracks, by applying the box-counting method and plotting $\log N(r)$ vs. $\log r$, there will be only one slope to report as the fractal dimension, which is constant (equal to unity); thus, other fractal dimensions, like an extended fractal dimension that captures the visual complexity of a pattern, could be more useful and should be explored in future works.

Acknowledgments

References

1.   FEMA 306. Evaluation of earthquake damaged concrete and masonry wall buildings, basic procedures manual. Washington (DC): The Patnership for Response and Recovery; 1998. https://www.fema.gov/media-library/assets/documents/3068. Accessed February 13, 2020.

2.   Hartle RA. Bridge Inspector's Reference Manual (BIRM). US Department of Transportation, Federal Highway Administration; 2002. https://www.fhwa.dot.gov/bridge/nbis.cfm. Accessed February 13, 2020.

3.   FEMA 307. Evaluation of earthquake damaged concrete and masonry wall buildings, technical resources. Washington (DC): The Patnership for Response and Recovery; 1998. https://www.fema.gov/media-library/assets/documents/3073. Accessed February 13, 2020.

4.   Dung CV, Anh LD. Autonomous concrete crack detection using deep fully convolutional neural network. *Automation in Construction*. 2019;99:52-58. doi:https://doi.org/10.1016/j.autcon.2018.11.028.

5.   Zou Q, Zhang Z, Li Q, et al. DeepCrack : Learning Hierarchical Convolutional Features for Crack Detection. *IEEE Transactions on Image Processing*. 2019;28(3):1498-1512. doi:10.1109/TIP.2018.2878966.

6.   Huyan J, Li W, Tighe S, Zhai J, Xu Z, Chen Y. Detection of sealed and unsealed cracks with complex backgrounds using deep convolutional neural network. *Automation in Construction*. 2019;107:102946. doi:https://doi.org/10.1016/j.autcon.2019.102946.

7.   Liu Z, Cao Y, Wang Y, Wang W. Computer vision-based concrete crack detection using U-net fully convolutional networks. *Automation in Construction*. 2019;104:129-139. doi:https://doi.org/10.1016/j.autcon.2019.04.005.

8.   Hoang N, Nguyen Q, Tran V-D, Nhat-Duc H, Nguyen Q, Tran V-D. Automatic recognition of asphalt pavement cracks using metaheuristic optimized edge detection algorithms and convolution neural network. *Automation in Construction*. 2018;94(July):203-213. doi:https://doi.org/10.1016/j.autcon.2018.07.008.

9.   Zhu Z, German S, Brilakis I. Visual retrieval of concrete crack properties for automated post-earthquake structural safety evaluation. *Automation in Construction*. 2011;20(7):874-883. doi:https://doi.org/10.1016/j.autcon.2011.03.004.

10.   Adhikari RS, Moselhi O, Bagchi A. Image-based retrieval of concrete crack properties for bridge inspection. *Automation in Construction*. 2014;39:180-194. doi:https://doi.org/10.1016/j.autcon.2013.06.011.

11.	Carpinteri A, Chiaia B, Nemati KM. Complex fracture energy dissipation in concrete under different loading conditions. *Mechanics of Materials*. 1997;26(2):93-108. doi:https://doi.org/10.1016/S0167-6636(97)00022-7.

12.	Carpinteri A, Corrado M, Lacidogna G. Three different approaches for damage domain characterization in disordered materials: Fractal energy density, b-value statistics, renormalization group theory. *Mechanics of Materials*. 2012;53(Supplement C):15-28. doi:https://doi.org/10.1016/j.mechmat.2012.05.004.

13.	Carpinteri A, Yang GP. Fractal dimension evolution of microcrack net in disordered materials. *Theoretical and Applied Fracture Mechanics*. 1996;25(1):73-81. doi:https://doi.org/10.1016/0167-8442(96)00009-2.

14.	Maosen C, Qingwen R, Pizhong Q. Nondestructive Assessment of Reinforced Concrete Structures Based on Fractal Damage Characteristic Factors. *Journal of Engineering Mechanics*. 2006;132(9):924-931. doi:10.1061/(ASCE)0733-9399(2006)132:9(924).

15.	Yang W, He X, Dai L. Damage behaviour of concrete beams reinforced with GFRP bars. *Composite Structures*. 2017;161(Supplement C):173-186. doi:https://doi.org/10.1016/j.compstruct.2016.11.041.

16.	Chiaia B, van Mier JGM, Vervuurt A. Crack Growth Mechanisms in Four Different Concretes: Microscopic Observations and Fractal Analysis. *Cement and Concrete Research*. 1998;28(1):103-114. doi:https://doi.org/10.1016/S0008-8846(97)00221-4.

17.	Adhikari SR, Moselhi O, Bagchi A, Rahmatian A. Tracking of Defects in Reinforced Concrete Bridges Using Digital Images. *Journal of Computing in Civil Engineering*. 2016;30(5):4016004. doi:10.1061/(ASCE)CP.1943-5487.0000566.

18.	Arvin E, Apostolos A, D. HT, Oguzhan B, Salvatore S. Fractal and Multifractal Analysis of Crack Patterns in Prestressed Concrete Girders. *Journal of Bridge Engineering*. 2019;24(7):4019059. doi:10.1061/(ASCE)BE.1943-5592.0001427.

19.	Athanasiou A, Ebrahimkhanlou A, Zaborac J, Hrynyk T, Salamone S. A machine learning approach based on multifractal features for crack assessment of reinforced concrete shells. *Computer-Aided Civil and Infrastructure Engineering*. November 2019. doi:10.1111/mice.12509.

20.	Momeni H, Dolatshahi KM. Predictive equations for drift ratio and damage assessment of RC shear walls using surface crack patterns. *Engineering Structures*. 2019;190:410-421. doi:https://doi.org/10.1016/j.engstruct.2019.04.018.

21.	Ebrahimkhanlou A, Farhidzadeh A, Salamone S. Multifractal analysis of crack patterns in reinforced concrete shear walls. *Structural Health Monitoring*. 2016;15(1):81-92. doi:10.1177/1475921715624502.

22.	Farhidzadeh A, Dehghan-Niri E, Moustafa A, Salamone S, Whittaker A. Damage Assessment of Reinforced Concrete Structures Using Fractal Analysis of Residual Crack Patterns. *Experimental Mechanics*. 2013;53(9):1607-1619. doi:10.1007/s11340-013-9769-7.

23.	Hilbert D. Ueber die stetige Abbildung einer Line auf ein Flächenstück. *Mathematische Annalen*. 1891;38(3):459-460. doi:10.1007/BF01199431.

24.	Sierpinski W. Sur une courbe cantorienne qui contient une image biunivoque et continue de toute courbe donnée. *CR Acad Sci Paris*. 1916;162:629-632.

25.	Julia G. Memoire sur l'iteration des fonctions rationnelles. *J Math Pures Appl*. 1918;7(4):47-245. http://eudml.org/doc/234994.

26.	Hausdorff F. Dimension und äußeres Maß. *Mathematische Annalen*. 1919;79(1):157-179. http://eudml.org/doc/158784.

27.	Richardson LF. The problem of contiguity: an appendix to statistics of deadly quarrels. *General systems yearbook*. 1961;6:139-187.

28.	Mandelbrot BB. *The Fractal Geometry of Nature*. New York: Freeman; ISBN:0-7167-1186-9; 1982.

29.	Peitgen H-O, Jürgens H, Saupe D. *Chaos and Fractals: New Frontiers of Science*. New York, NY, USA: Springer Science & Business Media; ISBN:0387218238; 2006.

30.   Corbit JD, Garbary DJ. Fractal Dimension as a Quantitative Measure of Complexity in Plant Development. *Proceedings: Biological Sciences*. 1995;262(1363):1-6. doi:https://doi.org/10.1098/rspb.1995.0168.

31.   Bouda M, Caplan JS, Saiers JE. Box-Counting Dimension Revisited: Presenting an Efficient Method of Minimizing Quantization Error and an Assessment of the Self-Similarity of Structural Root Systems. *Frontiers in Plant Science*. 2016;7:149. doi:https://doi.org/10.3389/fpls.2016.00149.

32.   Berntson GM. Root Systems and Fractals: How Reliable are Calculations of Fractal Dimensions? *Annals of Botany*. 1994;73(3):281-284. doi:https://doi.org/10.1006/anbo.1994.1033.

33.   Di Ieva A. *The Fractal Geometry of the Brain*. Springer; ISBN:978-1-4939-3995-4; 2016. https://link.springer.com/book/10.1007%2F978-1-4939-3995-4.

34.   Ostwald MJ. The Fractal Analysis of Architecture: Calibrating the Box-Counting Method Using Scaling Coefficient and Grid Disposition Variables. *Environment and Planning B: Planning and Design*. 2013;40(4):644-663. doi:https://doi.org/10.1068/b38124.

35.   Torre IG, Losada JC, Tarquis AM. Multiscaling properties of soil images. *Biosystems Engineering*. 2016. doi:https://doi.org/10.1016/j.biosystemseng.2016.11.006.

36.   Roy A, Perfect E. Lacunarity Analyses of Multifractal and Natural Grayscale Patterns. *Fractals*. 2014;22(03):1440003. doi:https://doi.org/10.1142/S0218348X14400039.

37.   Dathe A, Tarquis AM, Perrier E. Multifractal analysis of the pore- and solid-phases in binary two-dimensional images of natural porous structures. *Geoderma*. 2006;134(3):318-326. doi:https://doi.org/10.1016/j.geoderma.2006.03.024.

38.   Carrillo J, Avila W. Assessment of seismic damage of thin and lightly reinforced concrete walls using fractal dimension of cracking. *Earthquake Engineering & Structural Dynamics*. 2017;46(4):661-675. doi:10.1002/eqe.2808.

39.   Sandau K. A note on fractal sets and the measurement of fractal dimension. *Physica A: Statistical Mechanics and its Applications*. 1996;233(1):1-18. doi:https://doi.org/10.1016/S0378-4371(96)00248-8.

40.   Di Ieva A, Grizzi F, Ceva-Grimaldi G, et al. Fractal dimension as a quantitator of the microvasculature of normal and adenomatous pituitary tissue. *Journal of Anatomy*. 2007;211(5):673-680. doi:10.1111/j.1469-7580.2007.00804.x.

41.   Mandelbrot B. How long is the coast of Britain? Statistical self-similarity and fractional dimension. *science*. 1967;156(3775):636-638. doi:10.1126/science.156.3775.636.

42.   Feldman DP. *Chaos and Fractals: An Elementary Introduction*. Oxford: Oxford University Press; ISBN:0199566437; 2012.

43.   Carrillo J, Dominguez D, Prado N. Seismic Damage Index Based on Fractal Dimension of Cracking on Thin Reinforced Concrete Walls. *ACI Structural Journal*. 2017;114(6):1649-1658. doi:10.14359/51700919.

44.   Dolatshahi KM, Beyer K. Stiffness and Strength Estimation of Damaged Unreinforced Masonry Walls Using Crack Pattern. *Journal of Earthquake Engineering*. 2019;0(0):1-20. doi:10.1080/13632469.2019.1693446.

45.   Lopes R, Betrouni N. Fractal and multifractal analysis: A review. *Medical Image Analysis*. 2009;13(4):634-649. doi:https://doi.org/10.1016/j.media.2009.05.003.

46.   Allain C, Cloitre M. Characterizing the lacunarity of random and deterministic fractal sets. *PHYSICAL REVIEW A*. 1991;44(6):3552-3558. doi:10.1103/PhysRevA.44.3552.

47.   Plotnick RE, Gardner RH, O'Neill R V. Lacunarity indices as measures of landscape texture. *Landscape Ecology*. 1993;8(3):201-211. doi:https://doi.org/10.1007/BF00125351.

48.   de Melo RHC, Conci A. How Succolarity could be used as another fractal measure in image analysis. *Telecommunication Systems*. 2013;52(3):1643-1655. doi:10.1007/s11235-011-9657-3.

49.   Almeida J, Prodan O, Rosso A, Beyer K. Tests on Thin Reinforced Concrete Walls Subjected to In-Plane

and Out-of-Plane Cyclic Loading. *Earthquake Spectra*. 2016;33(1):323-345. doi:10.1193/101915EQS154DP.

50.   Falconer K. *Fractal Geometry: Mathematical Foundations and Applications*. Chichester: John Wiley & Sons; ISBN:0470871350; 2004.

51.   Ristanović D, Stefanović BD, Puškaš N. Fractal analysis of dendrite morphology using modified box-counting method. *Neuroscience Research*. 2014;84:64-67. doi:https://doi.org/10.1016/j.neures.2014.04.005.

52.   So G-B, So H-R, Jin G-G. Enhancement of the Box-Counting Algorithm for fractal dimension estimation. *Pattern Recognition Letters*. 2017;98(Supplement C):53-58. doi:https://doi.org/10.1016/j.patrec.2017.08.022.

53.   Foroutan-pour K, Dutilleul P, Smith DL. Advances in the implementation of the box-counting method of fractal dimension estimation. *Applied Mathematics and Computation*. 1999;105(2):195-210. doi:https://doi.org/10.1016/S0096-3003(98)10096-6.

54.   Da Silva D, Boudon F, Godin C, Puech O, Smith C, Sinoquet H. A Critical Appraisal of the Box Counting Method to Assess the Fractal Dimension of Tree Crowns. In: Bebis G, Boyle R, Parvin B, et al., eds. *Advances in Visual Computing: Second International Symposium, ISVC 2006 Lake Tahoe, NV, USA, November 6-8, 2006 Proceedings, Part I*. Berlin, Heidelberg: Springer Berlin Heidelberg; 2006:751-760. doi:10.1007/11919476_75.

55.   Roy A, Perfect E, Dunne WM, McKay LD. Fractal characterization of fracture networks: An improved box-counting technique. *Journal of Geophysical Research: Solid Earth*. 2007;112(B12). doi:10.1029/2006JB004582.

56.   Buczkowski S, Kyriacos S, Nekka F, Cartilier Lo. The modified box-counting method: Analysis of some characteristic parameters. *Pattern Recognition*. 1998;31(4):411-418. doi:https://doi.org/10.1016/S0031-3203(97)00054-X.

57.   Harrar K, Hamami L. Implementation of the box-counting method in radiographic images. In: Mastorakis N, Sakellaris J, eds. *Advances in Numerical Methods*. Boston, MA: Springer US; 2009:299-311. doi:10.1007/978-0-387-76483-2_26.

58.   Hou X-J, Gilmore R, Mindlin GB, Solari HG. An efficient algorithm for fast O($*$ln(N)) box counting. *Physics Letters A*. 1990;151(1):43-46. doi:https://doi.org/10.1016/0375-9601(90)90844-E.

59.   Petry S, Beyer K. Cyclic test data of six unreinforced masonry walls with different boundary conditions. *Earthquake Spectra*. 2015;31(4):2459-2484.

60.   Petry S, Beyer K. Scaling unreinforced masonry for reduced-scale seismic testing. *Bulletin of Earthquake Engineering*. 2014;12(6):2557-2581. doi:10.1007/s10518-014-9605-1.

61.   Karperien A. FracLac for ImageJ-FracLac Advanced User's Manual. Charles Sturt University, Australia. https://www.researchgate.net/publication/238733659_FracLac_Advanced_User's_Manual. Published 2007. Accessed February 13, 2020.

62.   Kaye BH. *A Random Walk through Fractal Dimensions*. John Wiley & Sons; ISBN:3527615989; 2008.

63.   Carpinteri A, Lacidogna G, Niccolini G, Puzzi S. Morphological Fractal Dimension Versus Power-law Exponent in the Scaling of Damaged Media. *International Journal of Damage Mechanics*. 2008;18(3):259-282. doi:10.1177/1056789508098700.

64.   Gonzato G, Mulargia F, Ciccotti M. Measuring the fractal dimensions of ideal and actual objects: implications for application in geology and geophysics. *Geophysical Journal International*. 2000;142(1):108-116. http://dx.doi.org/10.1046/j.1365-246x.2000.00133.x.

65.   AutoCAD Civil 3D, student version, Copyright © 2012 Autodesk, Inc. http://students.autodesk.com/ 2011.

66.   Pruess SA. Some Remarks on the Numerical Estimation of Fractal Dimension. In: Barton CC, La Pointe PR, eds. *Fractals in the Earth Sciences*. Boston, MA: Springer US; 1995:65-75. doi:10.1007/978-1-4899-1397-5_3.

67.   Rasband WS. ImageJ. https://imagej.net/Welcome. Published 1997. Accessed February 13, 2020.

68.   Meisel L V, Johnson MA. Convergence of numerical box-counting and correlation integral multifractal analysis techniques. *Pattern Recognition*. 1997;30(9):1565-1570. doi:https://doi.org/10.1016/S0031-3203(96)00162-8.

69.   Gonzato G. A Practical Implementation of the Box Counting Algorithm. *Computers & Geosciences*. 1998;24(1):95-100. doi:10.1016/S0098-3004(98)00082-X.

70.   Koch HP. The concept of fractals in the pharmaceutical sciences. *Die Pharmazie*. 1993;48(9):643—659. http://europepmc.org/abstract/MED/8234397.

71.   Cooper J, Oskrochi R. Fractal Analysis of Street Vistas: A Potential Tool for Assessing Levels of Visual Variety in Everyday Street Scenes. *Environment and Planning B: Planning and Design*. 2008;35(2):349-363. doi:10.1068/b33081.

72.   TruSoft International Inc. Benoit™. 1.01. 1997, St. Petersburg, Florida, USA. https://www.trusoft-international.com/. Accessed February 13, 2020.

73.   Sandau K, Kurz H. Measuring fractal dimension and complexity — an alternative approach with an application. *Journal of Microscopy*. 1997;186(2):164-176. doi:10.1046/j.1365-2818.1997.1270685.x.